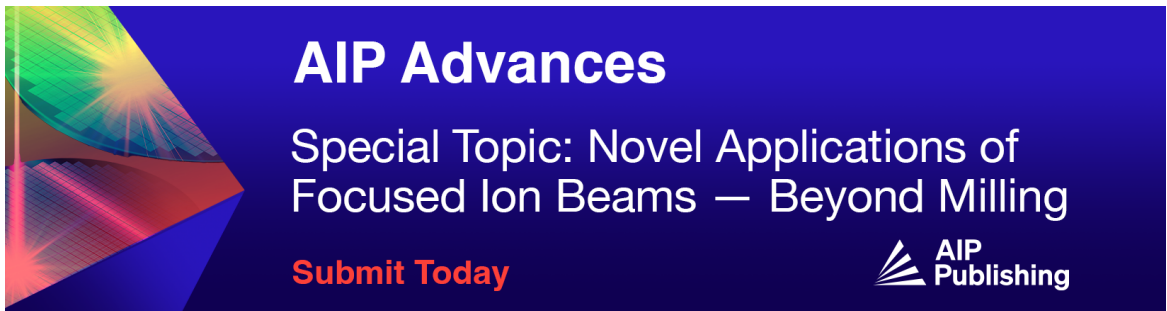# Nonlinear torsion-dominated deterioration behavior of wind generator output cable under electrothermal aging

Shuaibing Li ✉ 🔟 ; Baopeng Lu 🔟 ; Yi Cui 🔟 ; Yongqiang Kang 🔟 ; Haiying Dong

Check for updates

View Online   Export Citation

Nonlinear torsion-dominated deterioration behavior of wind generator output cable under electrothermal aging

View Online   Export Citation   CrossMark

Shuaibing Li,[1,2,a] (ID) **Baopeng Lu,**[2,b] (ID) **Yi Cui,**[3,c] (ID) **Yongqiang Kang,**[2,d] (ID) **and Haiying Dong**[2,e]

AFFILIATIONS

[1] National Rail Transit Electrification and Automation Engineering Technology Research Center, Chengdu 611756, Sichuan Province, China
[2] School of New Energy and Power Engineering, LanZhou Jiaotong University, 730070 Lanzhou, China
[3] School of Engineering, University of Southern Queensland, Springfield 4300, Australia

[a] Author to whom correspondence should be addressed: lishuaibing1105@163.com
[b] Electronic mail: lubaopeng0945@163.com
[c] Electronic mail: yi.cui@usq.edu.au
[d] Electronic mail: kangyong137@163.com
[e] Electronic mail: hydong@mail.lzjtu.cn

ABSTRACT

Wind turbine generator output cables are subjected to alternating torsional loads during long-term operation, combined with electrothermal stress, which may lead to insulation failure and other serious issues. Currently, the electrothermal aging mechanism under torsional stress is not fully understood. This study explores the synergistic degradation mechanism of electrothermal aging and nonlinear torsion by constructing a multi-stress aging test platform in the laboratory environment. This study involved accelerated aging tests with thermal, electrothermal, and electrothermal–torsional alternating stresses. The aged cable samples were analyzed for their physical and chemical properties using differential scanning calorimetry and Fourier transform infrared spectroscopy, while dielectric spectroscopy and mechanical tests were employed to evaluate their dielectric and mechanical performance. The results indicate that torsional stress induces physical changes at the molecular level in the ethylene–propylene rubber (EPR), leading to reduced strength, hardening, and increased brittleness, resulting in decreased mechanical strength. In addition, torsional stress promotes oxidation reactions and chain scission processes in the insulation layer, reducing crystallinity and causing a decline in mechanical performance. Increased oxidation and chain scission reactions result in an increase in polar groups, leading to an increase in the dielectric loss factor of the EPR. The findings of this study provide valuable insights for the design, manufacturing, and operational monitoring of wind turbine generator output cables.

I. INTRODUCTION

Wind power generation, as an important part of the carbon neutrality strategy, has seen rapid development in recent years due to its advantages such as large individual capacity and high utilization efficiency. As wind turbines move toward a larger capacity era, reliable power output has become an important indicator of the reliability of wind power generator sets. Currently, power cables with a rated voltage of 1.8/3.0 kV are commonly used for the power transmission from the generator inside the wind turbine nacelle to the tower base. The condition of these power cables is directly related to the safe operation of wind turbine units, and the operational reliability of the cables largely depends on the aging degree of the insulation.[1,2] Insulation aging severely limits the normal use of cables, so it is necessary to investigate the microscopic origin and evolution of aging during the service life of wind power cables and clarify the aging mechanism.[3,4]
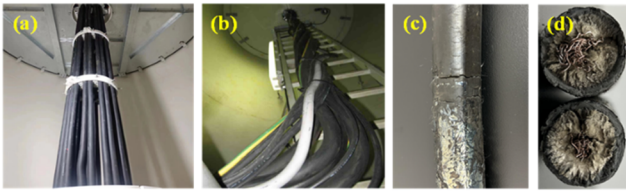
FIG. 1. The installation and torsional state of the power cables within the tower. (a) Cables suspension installation status. (b) Cables subjected to torsion state. (c) Twisted broken cable. (d) Cross section of twisted broken cable.

During the yawing process, the nacelle of the wind turbine must rotate according to changes in wind direction, causing the power cables to twist at a relatively high frequency. Figure 1 depicts the installation status of power cables for wind turbines inside the tower. In the event of an automatic cable release failure during yawing, the cable twist angle can exceed the 720° limit, leading to severe cable distortion. Additionally, since the cables are bundled and laid in the uppermost section of the tower, inadequate heat dissipation during operation can cause thermal aging of the cables. Therefore, Ethylene–Propylene Rubber (EPR) is widely used as the insulation material for power cables in wind turbines due to its excellent mechanical properties, electrical insulation performance, ozone resistance, chemical resistance, and flexibility.[5–7]

Studies have shown that cables are constantly subjected to electrical stress, thermal stress, and mechanical stress during operation. Due to continuous exposure to various stresses, the performance of cables begins to degrade, accelerating the aging process and shortening the cable's lifespan.[8] In the early stages, cables operated at lower voltage levels, and thermal effects were the main cause of insulation degradation.[9] After thermal-oxidative aging, EPR exhibits surface gasification and the presence of grooved areas, white block-like substances, and micropores on the surface. In addition, an increase in oxygen-containing groups, such as carbonyl groups, as well as free radicals of polyethylene and polypropylene are observed in the molecular structure. These changes have a significant impact on the electrical and mechanical properties of EPR.[10–13] Also, mechanical stress impacts electrical conductivity, dielectric breakdown strength, space charge behavior, and the initiation and propagation of branches in insulation materials.[14,15]

Studies reveals that cable insulation degradation accelerates significantly under multiple stress conditions, exhibiting synergistic effects that better reflect real-world application scenarios and operating environments of insulation materials.[16] Liu and Wang[17] observed that when subjected to combined electrical and mechanical stress, silicone rubber and EPR surfaces develop cracks and white products due to chain fracture and oxidation reactions. Specifically, Zhang et al.[18] studied the differences in mechanical properties, dielectric performance, and microstructure of XLPE insulation materials under single thermal aging and thermal-vibration combined effects. They analyzed the impact of vibration load on the insulation performance of cables.

The above-mentioned research findings have contributed to understanding the aging mechanisms of cables under multiple stress conditions. However, they do not sufficiently explain the insulation aging mechanisms of twisted power cables used in complex wind

turbine operating scenarios. This is primarily due to the following reasons:

(1) Existing research primarily focuses on aging EPR cable insulation under electrothermal stress, compression, and bending stress, without considering torsional loads.
(2) The stress levels experienced by EPR cables vary depending on the installation conditions.
(3) The aging mechanisms of EPR cables can differ based on their chemical compositions.
(4) Power cables in real-world operating conditions are subjected to significantly more complex conditions compared to laboratory settings, which may result in multiple aging mechanisms occurring simultaneously.

Therefore, this study aims to investigate the synergy degradation mechanism of wind power cable insulation under electrothermal aging and nonlinear torsion. To address this, a combined aging test platform was developed based on realistic operating conditions of wind power feeder cables. Various testing methods were used to obtain and analyze results under different aging modes. The mechanism behind the degradation of wind power cable insulation is discussed from different angles including mechanical, physical, and dielectric properties. The acceleration effect of nonlinear torsion load is uncovered and characterized through various measurements. The findings from this research will provide valuable insights into the influence of torsional loads on the long-term reliability of EPR cables. Moreover, these insights can guide the design, manufacturing, performance optimization, and operational monitoring of power cables specifically for wind turbines.

The organization of this article is as follows: Sec. II describes the cable sample preparation, aging stress settings, and analysis testing methods. Section III presents and elaborates on the measurement results. Section IV discusses the aging mechanisms. Section V provides the conclusions.

II. COMBINED DEGRADATION TEST OF WIND POWER CABLE

This paper adopts the method of accelerated aging test and utilizes a combined aging test platform consisting of a high-voltage test transformer, thermal-oxygen aging chamber, and torsion device to preproduce the electrical stress, thermal stress, and torsional loads during the yawing process of twisted power cables of wind generator. During the experiment, the insulation of the cable is subjected to a certain temperature and a constant electrical stress.

A. Experimental setup
1. Preparation of test cable samples

Figure 2(a) shows the electrothermal aging test platform, and Fig. 2(b) shows the torsion process of the cable is performed by the torsion testing machine, which secures the cable to the jaws on both ends of the revolving platform of the torsion testing machine. The test cables used are EPR cables with a rated voltage of 1.8/3 kV for wind power generators manufactured by Anhui Ansheng Special Cable Co., Ltd. in China. To ensure the accuracy of the test, the test cable is brand new and unused, with the model FDEF-25, cable specifications: single core, and conductor nominal cross-sectional area of
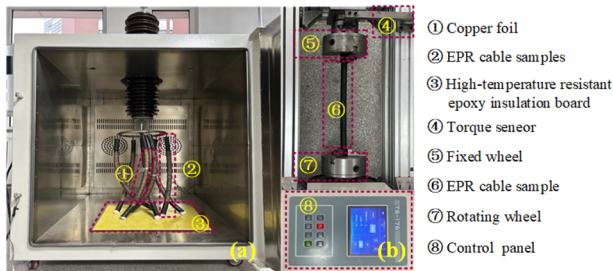
FIG. 2. Electrothermal–torsion combined aging test platform. (a) Electrothermal aging test chamber. (b) Torsion testing machine.

① Copper foil
② EPR cable samples
③ High-temperature resistant epoxy insulation board
④ Torque seneor
⑤ Fixed wheel
⑥ EPR cable sample
⑦ Rotating wheel
⑧ Control panel

TABLE I. Basic parameters of the wind power cable.

Structure name	Material	Outer diameter (mm)
Conductor	Copper	5.15
Insulation layer	Ethylene–propylene rubber	22.65
Outer sheath	Neoprene	29.08

TABLE II. Parameters of the partial discharge test transformer.

Model number	GY1013-50/100		
Rated capacity	50 kVA	Rated frequency	50 Hz
Rated voltage	0.4/100 kV	No-load current	4%
Rated current	125/0.5 A	Short-circuit impedance	9%
Cooling method	0NAN	Partial discharge quantity	<5 pC

20 mm^2. The relevant structural parameters are given in Table I. The right-side wheel of the torsion testing machine can rotate in both clockwise and counterclockwise directions, with adjustable angular velocity and angle. The torsion testing machine used is the N5010 wind power cable torsion testing machine produced by Jinan Xinbiao Automation Equipment Co., Ltd. in China. The sample cable is subjected to the rated voltage using a power frequency high-voltage test transformer produced by Jiangsu Yice Electric Power Equipment Co., Ltd. in China. The model and specific parameters of the transformer are given in Table II.

2. Experimental parameter settings

The experimental cables discussed in this paper were categorized into four groups: cables without aging treatment, thermally aged cables, cables subjected to electrothermal stress, and cables subjected to alternating electrothermal–torsional loads.

a. Thermal aging test. Based on the actual operating conditions of wind power cables and in accordance with the specifications of GB/T 29631-2013, EPR samples were aged through natural suspension. The samples were placed in a thermal-oxidative aging chamber to undergo accelerated thermal aging, with the test temperature set at 135 °C.

b. Electrothermal aging test. In accordance with GB/T 12706, the aging voltage was set at 7.2 kV, and the thermal aging temperature was maintained at 135 °C, with both electrical and thermal stresses applied simultaneously. The thermal-oxidative aging chamber was modified with an opening at the top to install a high-voltage bushing, enabling the safe introduction of alternating high voltage into the chamber. The upper end of the bushing served as the high-voltage input, while the lower end is connected to the cable sample as the output, equipped with a grading ring. During the test, ~5 cm of the insulation layer was stripped from one end of the cable to expose the conductor for high-voltage connection, while the other end remained untreated. The cable's outer sheath surface was cleaned with anhydrous ethanol to remove impurities, and then, a copper foil was tightly wrapped around the surface for grounding (the copper foil covered 40 cm of the cable length). The distance between the edges of the copper foil and the cable ends was 8 cm. To prevent discharge between the exposed conductor at the high-voltage end and the grounding electrode, the exposed conductor sections at both ends were sealed with high-temperature insulating adhesive after wiring.

c. Electrothermal–torsional aging test. The electrothermal–torsional aging test was conducted alternately between a thermal-oxidative aging chamber and a torsion testing machine. The torsion parameters were set as follows: both clockwise and counterclockwise torsion angles were 360°, with a torsion angular velocity of 720°/min. The process began with a 360° clockwise twist, followed by a 360° counterclockwise twist back to the initial position, then a 360° counterclockwise twist, and finally, a 360° clockwise twist back to the initial position, completing one full torsion cycle, which was then repeated. The electrothermal–torsional aging required alternating between the thermal-oxidative aging chamber and the torsion testing machine. For instance, for an aging duration of 168 h, the cable samples were first subjected to 168 h of electrothermal combined aging, followed by 168 h of torsional aging.

The aging durations for the three groups of samples were set at 168, 336, 504, 672, and 840 h. For clarity, the samples extracted from the three aging tests were labeled as t_aT, t_aET, and t_aETM, where "t_a" denotes the aging time in hours, "E" indicates the application of voltage during the test, "T" signifies thermal aging, and "M" represents the application of torsional load. Detailed experimental conditions and aging time settings are provided in Table III. Samples that did not undergo any aging treatment were used as the control group and were simply labeled as N.

TABLE III. Aging conditions and aging time settings.

Aging conditions and time	168 h	336 h	504 h	672 h	840 h
Thermal aging	t_{168}T	t_{336}T	t_{504}T	t_{672}T	t_{840}T
Electrothermal aging	t_{168}ET	t_{336}ET	t_{504}ET	t_{672}ET	t_{840}ET
Electro-thermal-torsion aging	t_{168}ETM	t_{336}ETM	t_{504}ETM	t_{672}ETM	t_{840}ETM

B. Methods for aging test analysis

Based on the insulation material type and application scenarios, evaluating cable insulation status typically involves measuring surface resistance, leakage current, partial discharge, and other characteristics. However, these test results only capture changes in electrical performance and lack detailed insights into the origin and progression of cable aging.[8] Consequently, numerous research teams have integrated physical and chemical analysis techniques, such as scanning electron microscopy, thermogravimetric analysis, differential scanning calorimetry, and infrared spectroscopy, to investigate insulation degradation mechanisms.

To comprehend the impact of various aging modes on the physical, chemical, mechanical, and dielectric properties of wind power cables, samples were collected from different cable positions at specific aging durations. These samples underwent analyses, such as infrared spectroscopy, differential scanning calorimetry, dielectric performance testing, elongation at break (EAB), and tensile strength testing. These testing methods serve to characterize the degradation characteristics of EPR cable insulation under different aging conditions.

1. Fourier transform infrared spectroscopy analysis (FTIR)

The changes in functional groups of EPR during different aging processes were analyzed using the TENSOR27 Fourier Transform Infrared Spectrometer produced by Bruker in Germany. The test wavenumber range was 4000–500 cm^{-1}, with a resolution of 0.5 cm^{-1}.

2. Differential scanning calorimetry analysis (DSC)

The Mettler–Toledo DSC3 Differential Scanning Calorimeter from Switzerland was used to quantitatively measure the melting enthalpy and crystallization performance of the cable samples under different aging conditions. The differences in crystallinity of the EPR cable samples under different aging conditions were compared. The test temperature range was 0–480 °C, with a heating and cooling rate of 10 °C/min, and the sample weight was 5–8 mg.

3. Dielectric performance testing

The Agilent 4294A Precision Impedance Analyzer was used to test the dielectric constant and dielectric loss tangent of the aged samples and to compare and analyze the changes in the insulation dielectric performance of the cable under different aging conditions and aging times. The test frequency range was 50–10^7 Hz.

4. EAB and tensile strength testing

Referring to GB/T 2951.11-2008/IEC 60811-1-1:2001, standard dumbbell-shaped specimens were prepared to test the tensile strength and f elongation at break of the cable samples. The sample was tested at a tensile speed of 200 mm/min and a testing temperature of (23 ± 2) °C. The experimental instrument used was the CMT-4503 electronic tensile testing machine.

III. TEST RESULTS ANALYSIS

A. FTIR analysis

The changes in the position, intensity, and shape of absorption peaks in infrared spectra can be used to reflect the variations in
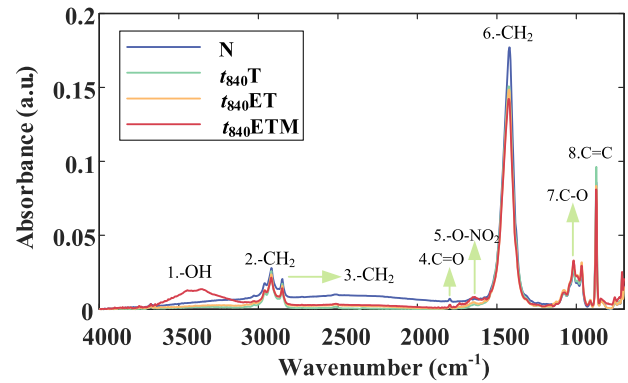

FIG. 3. Infrared spectra of aging of EPR cable insulation for wind turbines.

chemical groups within materials and qualitatively obtain the aging characteristics of materials. To investigate the influence of aging time and aging conditions on the EPR molecular structure, samples of the insulation layer of aged cables were taken, and attenuated total reflectance Fourier transform infrared spectroscopy (ATR-FTIR) was used to test and compare the infrared spectra of the samples. Typical infrared spectral features of the insulation layer of the cable were obtained, as shown in Fig. 3.

Absorption peaks corresponding to the deformation and stretching vibrations of –OH appeared in the range of 3100–3650 cm^{-1}, while peaks at 2916 and 2848 cm^{-1} were attributed to the symmetric and asymmetric stretching vibrations of –CH_2-groups.[19] An absorption peak associated with the symmetric stretching vibration of –O–NO_2 appeared in the range of 1650–1600 cm^{-1}. The absorption peak at 1733 cm^{-1} corresponds to the stretching vibration of C=O, while the absorption peaks at 1076 and 1017 cm^{-1} correspond to the C–O in esters/ethers. The presence of C=O in the unaged samples indicated oxidation reactions occurring during the manufacturing process, possibly due to curing reactions between the rubber matrix, sulfur, and other reagents.[20] The peak at 1125 cm^{-1} was attributed to the stretching vibration mode of C–O–C or the skeletal vibration mode of C–C.[21] The peak at 875 cm^{-1} belonged to an absorption band originating from the deformation vibration of C=C groups.[22] The results in Fig. 3 indicated significant changes in the absorption peaks of certain groups in the insulation layer after long-term exposure to thermal stress and electrothermal or electrothermal–torsional combined stresses. The absorption peaks in different wavenumber ranges within the characteristic region are shown in Fig. 4.

The appearance of peaks at 1650–1600 and 1733 cm^{-1} in Fig. 3 indicates that oxidation reactions occur in EPR during chain scission, resulting in the formation of nitroso and carbonyl groups. Among them, the variation of the C=O stretching vibration at 1733 cm^{-1} is most pronounced under the electrothermal–torsional aging condition. When C=O appears in EPR molecular chains, it indicates internal oxidation, an increase in polar groups within the sample, an increase in charge in the insulation, easier migration, and an increase in dipole polarization intensity. As shown in Figs. 4(a) and 4(b), compared to the unaged samples, the intensity of the characteristic absorption peaks at 2916, 2848, and 1421 cm^{-1} shows a
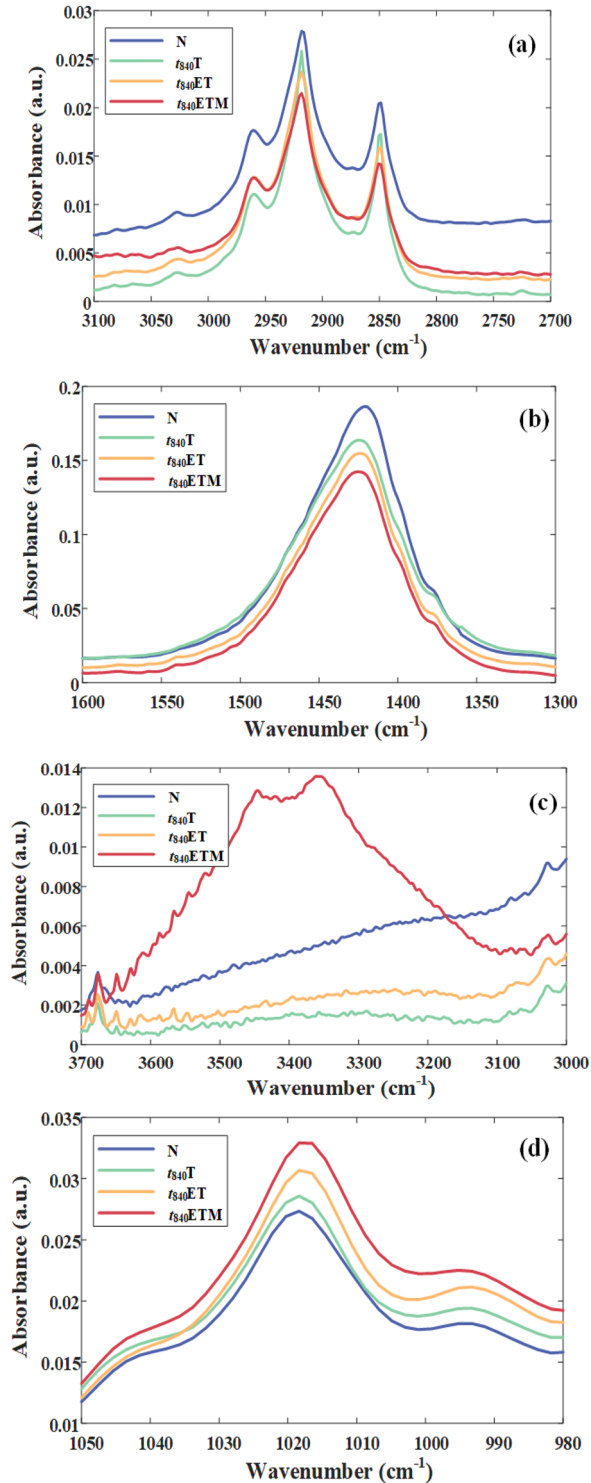
FIG. 4. Absorption peaks in different characteristic regions of the cable specimen. (a) Characteristic absorption peaks at 2916 and 2848 cm^{-1}. (b) Characteristic absorption peak at 1421 cm^{-1}. (c) Characteristic absorption peaks in the range of 3650–3100 cm^{-1}. (d) Characteristic absorption peak at 1017 cm^{-1}.

decreasing trend under the three different aging methods, confirming a decrease in the methyl content in EPR and indicating severe chain scission reactions in both the main chain and side chains during aging.[23,24]

Under the three different aging conditions, the intensities of the characteristic absorption peaks at 2916, 2848, and 1421 cm^{-1} satisfy the relationship: N > t840T > t840 ET > t840ETM, indicating that the superimposed aging stresses accelerate the chain scission process of the cable samples. In addition, the results in Figs. 4(c) and 4(d) show an increasing trend in the intensity of the characteristic absorption peaks at wavenumbers 3100–3650 and 1017 cm^{-1} under the three different aging methods. The enhancement of the C–O characteristic peak suggests that large molecular chains in EPR undergo degradation reactions involving chain breakage, formation of carbon radicals, oxidation reactions, and the formation of numerous C–O bonds. The intensity changes in the absorption peaks indicate that torsional loads promote chain scission and oxidation reactions in EPR to some extent.

At high temperatures, the double bond structure in EPR rubber is susceptible to thermal cracking reactions, leading to the formation of C=O and C–O. In addition, the molecular structure of EPR rubber undergoes changes under the influence of an electric field, resulting in the creation of C=O. The research by Liu *et al.* indicates that both electrical aging and electro-mechanical aging can alter the absorption peak of C=O in EPR, attributed to bond cleavage, oxidation reactions, and the formation of C–O bonds.[16] Notably, the infrared spectroscopy results from the three aging test groups revealed no emergence of new functional groups during the aging process. The perspective presented in this paper suggests that during thermal aging and electrothermal aging, EPR rubber experiences both bond cleavage and oxidation reactions, leading to the formation of C=O and C–O, consequently deteriorating its mechanical properties. Furthermore, repetitive twisting can induce fatigue aging in cables. When subjected to coupled stress, twisting stress accelerates bond cleavage and oxidation reactions by disrupting hydrogen bonds and weakening molecular entanglement, resulting in the generation of more C–O or C=O, without altering the reaction mechanism or product types.

To further characterize the effects of different aging conditions on the molecular chains of the samples, the carbonyl index is defined to represent the degree of aging of the samples. Since the absorption intensity of the peak at 1370 cm^{-1} changes only slightly during the aging process, the ratio of the intensity of the absorption peak at 1733 cm^{-1} to the intensity of the absorption peak at 1370 cm^{-1} is defined as the carbonyl index,[19]

$$C = \frac{I_{1733}}{I_{1370}}. \quad (1)$$

The carbonyl indices of samples with different aging degrees are given in Table IV.

From Table IV, it can be observed that under the same aging conditions, the carbonyl index gradually increases with the prolongation of aging time. Under the same aging time, the more complex the aging conditions, the higher the carbonyl index. It is worth noting that the difference in carbonyl index between thermal aging and electrothermal aging conditions in cable samples is small, while

TABLE IV. Carbonyl indices of aged samples.

Aging conditions/aging time	168 h	504 h	840 h
Thermal aging	0.0179	0.0190	0.0219
Electrothermal aging	0.0234	0.0341	0.0410
Electrothermal-torsion aging	0.0630	0.1356	0.1492

the carbonyl index value of the electrothermal–torsion test group is significantly higher than the other two aging test groups.

B. DSC analysis

Further investigation of the morphological changes in EPR samples during the aging process was carried out using a differential scanning calorimeter.[25] The changes in the exothermic curves of the measured samples were analyzed by DSC for a comparative analysis of the aged samples, as shown in Fig. 5.

From Fig. 5, it can be observed that the melting curve contains two distinct exothermic regions, forming two peaks. The presence of these two peaks is due to the existence of two compounds with different melting temperatures in the cable samples, leading to selective crystallization of different molecular weight components and
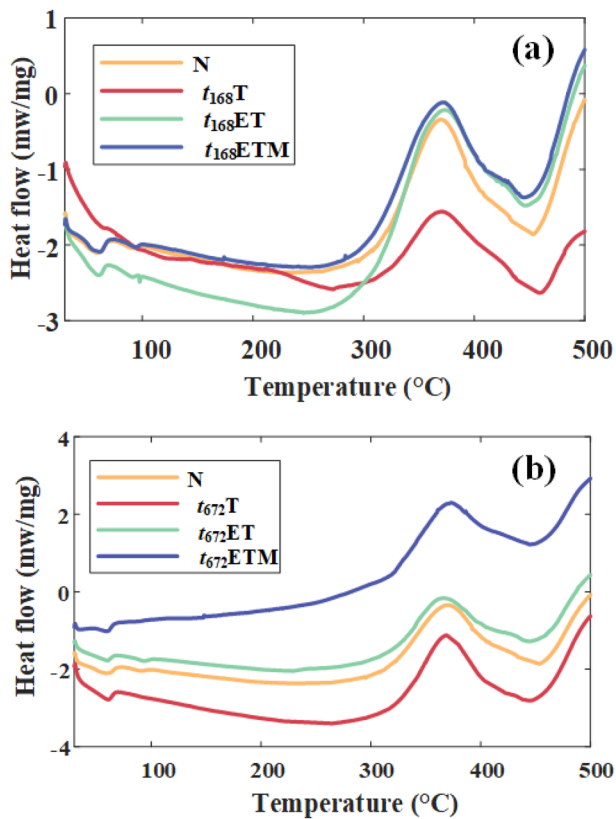

FIG. 5. DSC curves of specimens with different aging times and aging conditions. (a) t = 168 h, (b) t = 672 h.

resulting in two distinct melting peaks.[26–28] The DSC analysis in this article focuses on the main peak.

The heat absorption values of EPR samples under different aging times and conditions were obtained by integrating the main peak region of the DSC curves. The crystallinity of the samples was then calculated using the following equation (2) (results are given in Table V):

$$X_c = \frac{\Delta H}{\Delta H_0} \times 100\%, \tag{2}$$

where X_c represents the crystallinity of the material, ΔH is the enthalpy obtained from the DSC curve, and ΔH_0 is the enthalpy of the material at 100% crystallinity (270 J/g for EPR).[19]

From Table V, it can be seen that the melting temperature of the samples exhibits a trend of initially increasing and then decreasing. According to the calculated results of the crystallinity of the samples, it is evident that the crystallinity decreases under different aging conditions at an aging time of 168 h. At an aging time of 672 h, the crystallinity increases for samples subjected to thermal aging and electrothermal aging, while the crystallinity decreases by 17.46% for samples under the electrothermal–torsion aging condition. This behavior indicates that during the initial stages of aging, both chemical bond breakage and further cross-linking of EPR occur within the insulation material, resulting in an increase in crystallinity.

To further investigate the influence of torsional stress on its thermal performance, the DSC results of samples subjected to electrothermal–torsion stress at different times were analyzed, as shown in Fig. 6. After 168 h of electrothermal–torsion aging, a melting peak is formed near 445.91 °C, with a rightward shift of the melting peak. For the remaining samples, there is a trend of leftward shift of the melting peak temperature as the aging time progress, indicating a gradual decrease in heat resistance.

According to Table V, under the aging condition of electrothermal–torsion, when the aging time is 168 h, the crystallinity of the sample decreases to 29.13%. When the aging time is 672 h, EPR undergoes further cross-linking under high temperature, and the crystal structure tends to be improved, with the crystallinity increasing to 34.12% and 30.58%, respectively. Under the electrothermal–torsion condition, the crystallinity drops sharply to 22.77%. This is because under the action of torsional stress, the long polymer chains in the sample undergo orientation, slip, and recrystallization, resulting in a change in crystallinity. Various stress effects cause the breakage of polymer chains, resulting in the shearing of chain segments into smaller segments, an increase in short side chains, and the generation of more chain breaks and oxidation products, leading to a significant decrease in crystallinity and a decrease in crystallization ability.[21] The reason for the increase in crystallinity during the aging process may be that the breakage of polymer chains in EPR disrupts the entangled network, and the small chain segments produced have strong activity, which can undergo secondary crystallization along the original grain boundaries, resulting in an increase in crystallinity.

C. Dielectric performance testing

To investigate the changes in the dielectric performance of the insulation layer of a cable under different aging stress, the aged cable samples were subjected to comparative testing of dielectric

TABLE V. Calculation results of crystallinity of samples in different aging states.

Sample	Onset temperature of melting peak (°C)	Onset temperature of melting peak (°C)	Enthalpy of fusion ΔH (J/g)	Melting temperature T_m (°C)	Crystallinity X_c (%)
N	387.16	490.28	82	453.21	30.37
t_{168}T	408.81	484.91	66.42	458.98	24.6
t_{168}ET	383.63	483.4	62.02	446.73	22.97
t_{168}ETM	385.82	479.82	78.65	445.91	29.13
t_{672}T	375.66	487.88	92.12	444.97	34.12
t_{672}ET	392.54	489.41	82.57	445.58	30.58
t_{672}ETM	383.59	477.12	47.13	444.08	17.46
t_{336}ETM	374.55	449.33	97.10	445.08	35.96
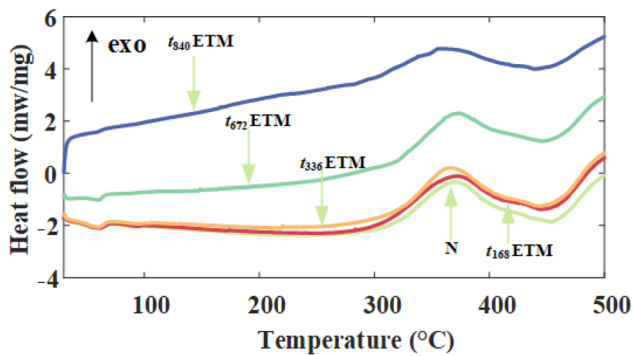
FIG. 6. DSC curves of specimens with different aging times during electrothermal–torsional aging.

loss. The obtained dielectric loss factor test curves are shown in Figs. 7(a)–7(c).

From Fig. 7, it can be seen that the variation process of the dielectric loss values of the samples under three different aging conditions with increasing frequency is basically similar. Under the same aging condition and aging time, the dielectric loss value gradually decreases with increasing frequency. Under the same aging condition, the dielectric loss value shows an upward trend with increasing aging time. The dielectric loss values gradually tend to be consistent after the frequency exceeds 10^3.

To compare the characteristics of the effects of different aging conditions on the cable's dielectric performance, we integrated the frequency–dielectric loss curves within the range of 50–10^3 Hz, the point value is represented by Z, and the results are shown in Fig. 7(d). It can be seen from Fig. 7(d) that under the same aging time, the integration value of the electrothermal–torsional aging sample is larger than that of the electrothermal aging sample, while the integration value of the single thermal aging sample is the smallest. With the increase of aging time, the difference in integration values among the three aging conditions gradually increases. The test results of the dielectric loss indicate that electrical stress and mechanical stress will promote the deterioration process of the dielectric performance of wind power cables.
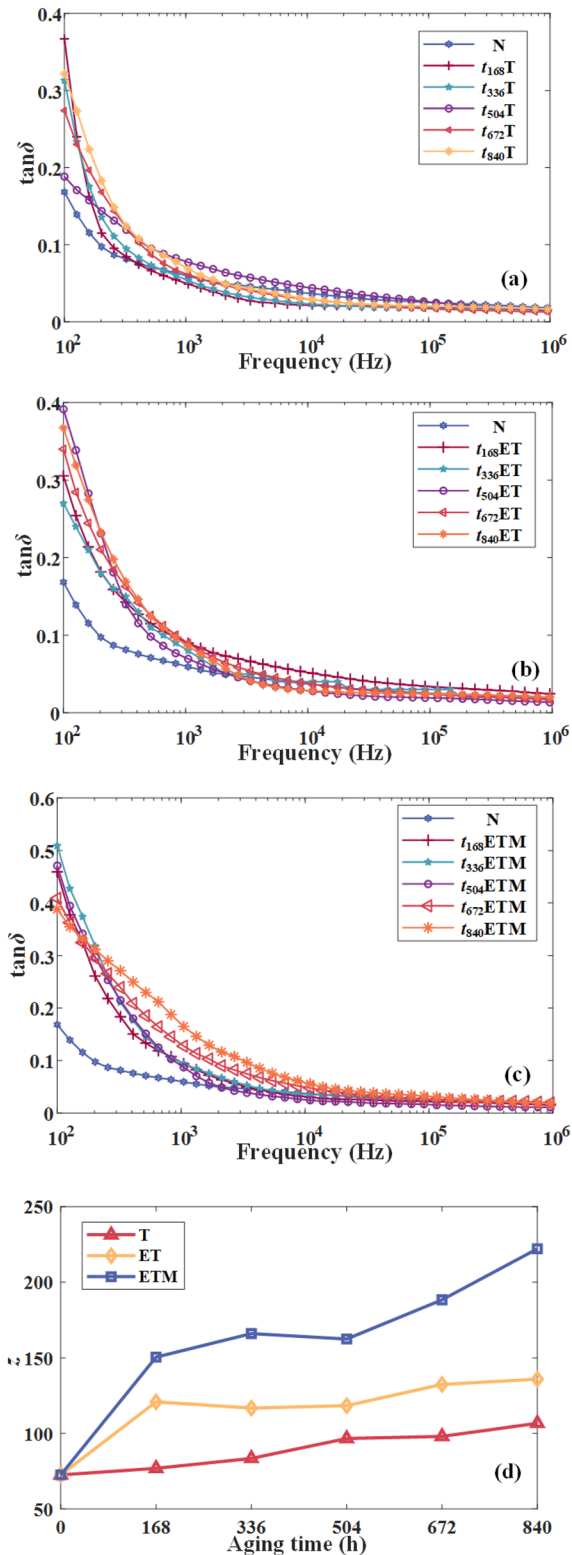
D. EAB and tensile strength testing

The EAB and tensile strength can reflect the mechanical properties of the cable after accelerated aging. Samples were taken from different positions of the cable insulation and standard dumbbell-shaped specimens were prepared for mechanical performance testing. The fracture growth rate and tensile strength of the samples under different aging times and conditions are shown in Figs. 8 and 9, respectively.

Under all three aging conditions, the EAB and tensile strength of the cable samples decrease as the aging time increases. However, the decrease in EAB is not significant at 168 and 336 h of aging, and the impact of the three aging conditions on the mechanical performance is similar. Analysis of the crystallinity reveals that under short-term high temperature, the crystallinity of EPR slightly increases, leading to an improvement in the crystalline structure without significant degradation in the mechanical properties of the cable insulation. However, at aging times of 672 and 840 h, a noticeable decrease in the mechanical performance is observed. At an aging time of 840 h, the EAB of the samples under thermal, electrothermal, and electrothermal–torsional aging conditions are measured as follows: 407%, 402%, and 371%, respectively. The rate of decrease in EAB and tensile strength is significantly accelerated under the electrothermal–torsional aging condition. The degradation of mechanical properties under thermal stress may be attributed to the precipitation of additives in the samples under thermal-oxygen conditions. Meanwhile, electrical stress can induce chain scission reactions and the formation of "microcracks" within the samples.[29]

For limitations in the production process, there are tiny voids in the EPR samples. Under electrical stress, high-energy particles generated by void discharges bombard the interior of the samples, leading to the breakage of main chains and the severing of side chains in the EPR molecules. On the basis of electrothermal aging, the addition of torsional stress promotes chain scission and oxidation reactions. This continuous expansion of tiny voids, along with the formation of more voids and the enlargement of existing voids, accelerates the chain breakage process. At the same time, torsional stress weakens the physical cross-linking and entanglement between EPR molecules and increases molecular activity and also the average distance between polymer chains. This facilitates chain exposure to

06 August 2024 05:03:50

FIG. 7. Dielectric loss of specimens in different aging states. (a) T. (b) ET. (c) ETM. (d) Frequency–dielectric loss curve integral value Z.
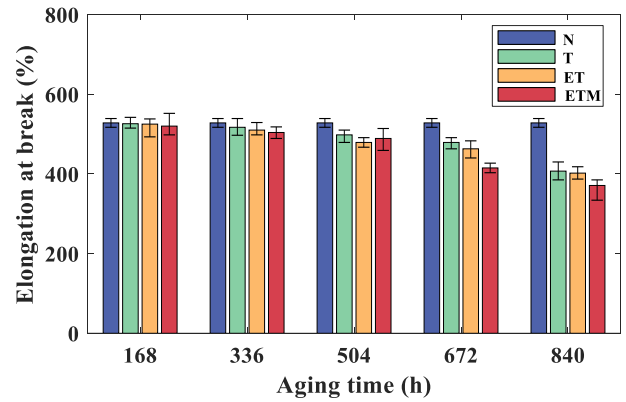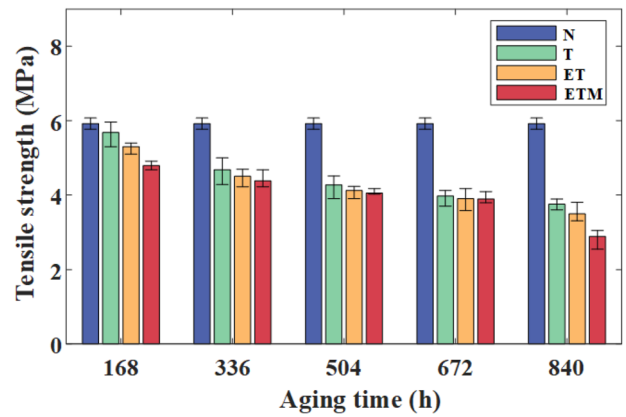

FIG. 8. EAB in different aging states.

FIG. 9. Tensile strength testing in different aging states.

discharge particles and oxidative environments, promoting oxidation reactions.

IV. ANALYSIS OF MULTI-STRESS AGING MECHANISM

A. Strain measurement during the cable twisting process

The Digital Image Correlation (DIC) three-dimensional strain measurement analysis system is utilized to analyze the surface strain of wind power cables during the torsion process. The measurement system, depicted in Fig. 10, operates on a simple principle: first, a validated calibration board is used to calibrate the binocular camera system and acquire the internal and external parameters of the two cameras; next, the correlation matching algorithm is employed to obtain the disparity data of corresponding points in the images captured by the left and right cameras; subsequently, the calibration parameters and disparity data are utilized to derive the three-dimensional surface morphology of the object; finally, by comparing the three-dimensional morphology changes of each point, the full-field three-dimensional displacement distribution and strain distribution are obtained.
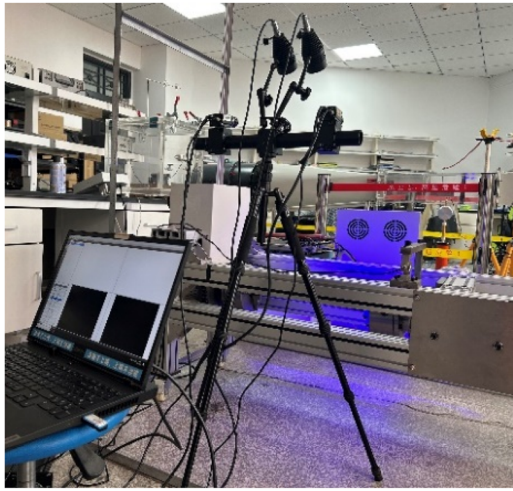
06 August 2024 05:03:50

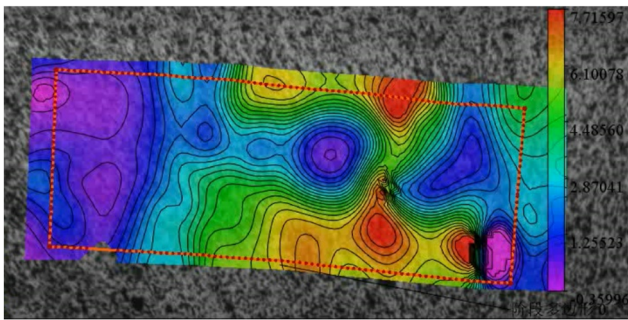FIG. 10. DIC three-dimensional strain measurement analysis system.

FIG. 11. Strain distribution on the surface of the cable test specimen.

For improved sampling, the cable twisting process is set as follows: clockwise and counterclockwise twisting at a 45° angle with a speed of 6 rpm. In Fig. 11, the strain distribution on the cable sample's surface after 840 h of electrothermal-twisting aging is depicted. It is evident from the figure that during the clockwise and counterclockwise twisting processes, the strain on the cable varies, resulting in local stress concentration. Measurements reveal that when the same part of the cable sample is subjected to clockwise and counterclockwise twisting loads, it experiences repeated alternating tensile and compressive stresses. As the cable ages, its strain capacity significantly diminishes. The repeated twisting stresses cause molecular chains to shift, slide against each other, and break, leading to a reduction in rubber strength, hardening, and embrittlement, ultimately resulting in a decline in mechanical performance.

B. Mechanism analysis of cable aging

Further analysis of the internal stress distribution in the cable was conducted, and the torque and shear stress distribution on the cross section of the cable specimen is shown in Fig. 12. It can be observed from Fig. 12 that the maximum shear stress occurs at
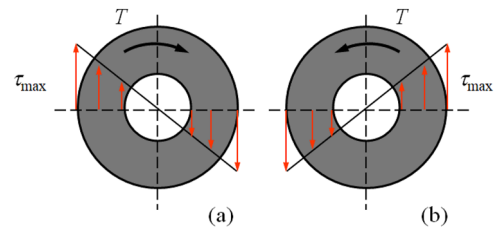

FIG. 12. Torsion and stress distribution in the cross section of cable. (a) Clockwise torsion. (b) Counterclockwise torsion.

the periphery of the section, which is the outer sheath part, and is perpendicular to the radius.

The thermal effects lead to changes in the molecular structure of the outer sheath and insulation layer of the cable, causing the hardening and embrittlement of the cable's outer sheath and insulation layer, and a gradual decrease in the material's elasticity. The torsional effect subjects the various layers of the cable to alternating compression and tension, resulting in compressive stress and tension. Under the alternating compressive and tensile forces, due to the increased brittleness of the material and the fatigue effects on the molecules, it is more likely for molecular chains to shift and break, leading to the gradual appearance of microcracks on the cable surface. The damage process is illustrated in Fig. 13.

The white portion represents the trend of microcrack development. Under the torsional effect, microcracks gradually form and continuously expand radially and axially. When subjected to torsional forces, the material's molecular structure cannot withstand external stress, leading to localized stress concentrations, thereby causing the formation of microcracks on the material surface. This phenomenon is commonly referred to as fatigue cracking, which occurs due to prolonged stress or degradation of the material resulting in decreased performance. The mechanical and physical properties of the main insulation of the wind turbine generator output cables far exceed those of the outer sheath, causing the outer sheath to crack under long-term torsional stress, promoting thermal oxygen permeation into the insulation, gradually leading to cracking of the insulation layer, affecting the electrical and mechanical performance of the cables.[29] Various aging stresses coexist during the normal operation of the cable, and these aging stresses can interact or synergistically act upon each other.
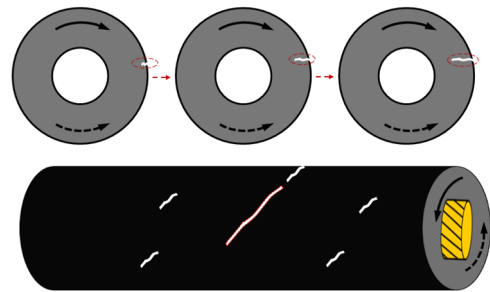

FIG. 13. Development process of internal and surface cracks in cable specimens.

06 August 2024 05:03:50

In a study involving the cable samples, they were cut into 1 mm thick slices and coated with gold before being scanned using a ZEISS Gemini SEM 500 scanning electron microscope from Carl Zeiss in Germany after 840 h. The tests on the cable samples' outer sheath and insulation layer revealed noteworthy findings, as depicted in Fig. 14. As per the results in Fig. 14, the surface of the non-aging cable outer sheath is smooth. However, thermal aging induces the appearance of cracks, and these cracks further expand under electrothermal aging and electrothermal–torsional conditions.

When EPR is subjected to repeated twisting, the hydrogen bonds and van der Waals bonds between the molecular chains are
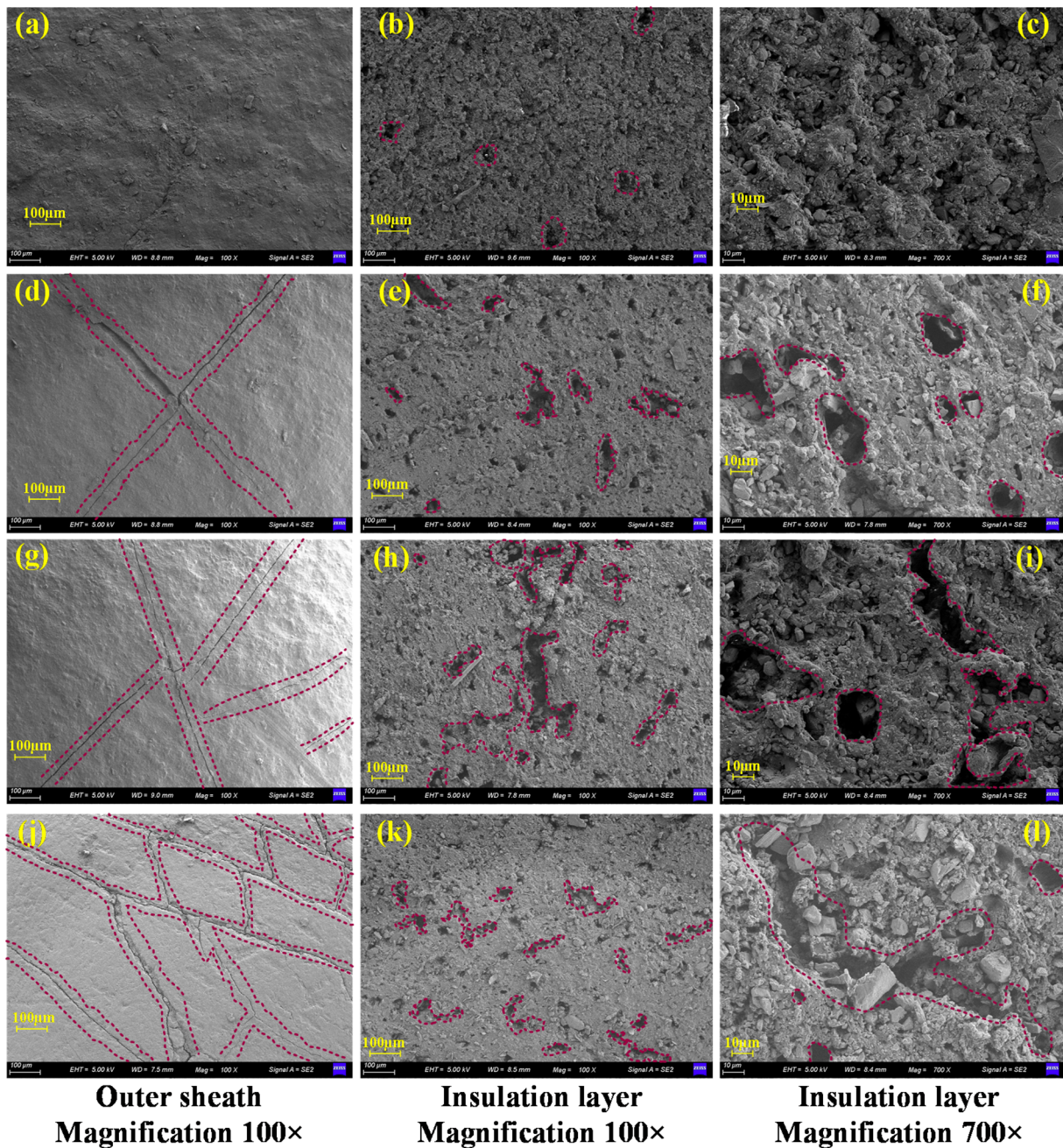

| Outer sheath | Insulation layer | Insulation layer |
| Magnification 100× | Magnification 100× | Magnification 700× |

FIG. 14. Micro-morphological analysis of specimen after aging for 840 h. (a)–(c) N. (d)–(f) T. (g)–(i) ET. (j)–(l) ETM.

initially broken, leading to an increase in stress concentration on the EPR rubber main chain. As the torsional stress reaches a certain threshold, some main molecular chains either directly break or become susceptible to breakage under high electric fields.[30] In the presence of an electric field, the thermal oxygen reaction contributes to chain breakage, resulting in the formation of unsaturated groups such as carbonyl groups and others. The mechanism of insulation failure in wind power cable samples is proposed based on experimental results. Under the influence of electric and thermal stress, both the main chain and side chains of EPR molecules experience chain breakage, leading to the production of alkyl radicals R• and •H. The alkyl radical R• undergoes an oxidation reaction and reacts with the hydrogen atoms of EPR to produce hydrogen peroxide (ROOH), which then decomposes into alkoxyl radicals RO and hydroxyl radicals •OH. The alkoxyl radical RO• further reacts with •H to produce RO-H or forms a carbonyl group (C=O) through β-scission. This explains the presence of –OH, C–O, and C=O on the surface of aged EPR samples. Under repeated torsional stress, the wind power cable insulation undergoes internal cyclic stress changes, leading to the expansion and aggregation of microcracks, ultimately resulting in material fatigue failure. The EPR rubber aging mechanism under torsion is illustrated in Fig. 15.

The equivalent circuit model for conducting dielectric performance tests on the samples is illustrated in Fig. 16. When an alternating voltage is applied to the cable sample, the internal current comprises two components: the displacement cur-rent I_C in the vacuum and the current I_P induced by the various polarization processes established within the dielectric,

$$\dot{I} = \dot{I}_P + \dot{I}_C, \tag{3}$$

$$I_P = \left(\gamma + \frac{\omega^2 \tau^2 g}{1 + \omega^2 \tau^2} \right) SE = (\gamma + g)\, SE, \tag{4}$$
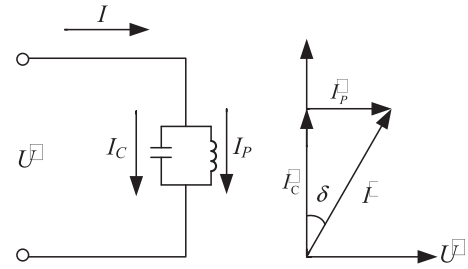

FIG. 16. The equivalent model and vector diagram for measuring the dielectric loss.

$$I_C = \omega \varepsilon_0 \varepsilon_r\, SE, \tag{5}$$

$$\tan \delta = \frac{I_P}{I_C} = \frac{\gamma + g}{\omega \varepsilon_0 \varepsilon_r}, \tag{6}$$

where γ represents the electrical conductivity of the dielectric, g is the equivalent conductivity of dielectric relaxation polarization loss, ε_0 is the vacuum permittivity, ε_r is the relative permittivity of the dielectric, ω is the test angular frequency, S is the equivalent area of the dielectric, and E is the average electric field strength of the dielectric. At low frequencies, g is significantly smaller than γ, and g can be considered negligible. Therefore, the conductivity determines the dielectric loss factor of the cable, as follows:

$$\tan \delta = \frac{\gamma}{\omega \varepsilon_0 \varepsilon_r}. \tag{7}$$

From Fig. 7, it is evident that within the $0–10^3$ Hz range, under the same aging conditions, the conductive loss decreases signifi-
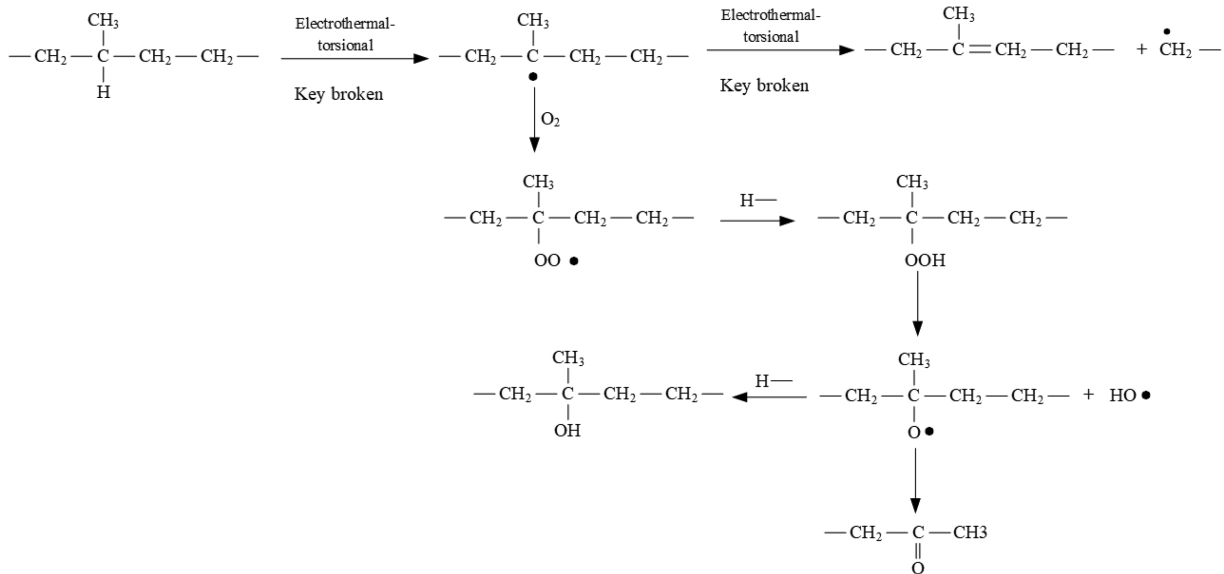

FIG. 15. EPR rubber aging mechanism under torsion.

cantly with increasing frequency. As the aging time increases, tan δ shows a gradual increasing trend. Similarly, under the same aging duration, tan δ also demonstrates a gradual increase, with the trend generally following T3 > T2 > T1. Beyond 10^4 Hz, tan δ tends to converge and gradually stabilize.

The main reason for the above phenomenon is as follows: On the one hand, the results from the infrared spectroscopy analysis indicate that torsional stress accelerates the fracture of chemical bonds and oxidation reactions by disrupting hydrogen bonds and weakening molecular entanglement. This process generates more small molecular groups and polar substances, such as oxidation products compared to thermal aging and electrical-thermal aging. These polar molecules increase the overall conductivity of the EPR molecules, leading to a gradual increase in the dielectric loss factor of the aged samples within the $0–10^3$ Hz range. On the other hand, prolonged torsion increases the distance between molecules within the insulation material, thereby reducing the resistance to electron movement within it.[31]

After 10^4 Hz, in the high-frequency range, the tan δ of the sample is primarily contributed by displacement polarization. During the aging process, the free radicals generated from the side chain breakage of EPR molecules exhibit partial ionic characteristics. The loss generated by polarization gradually increases with the aging degree of the sample. However, the increase in intermolecular gaps due to molecular chain breakage reduces the dielectric relaxation effect during polarization, leading to a corresponding decrease in loss. Therefore, the variation in tan δ in the high-frequency range of different aged samples is not significant.

V. CONCLUSIONS

This study focused on wind turbine generator output cables and established an electrothermal–torsional combined aging test platform to simulate the actual working conditions of the cables, revealing the promoting effect of torsional stress in the electrothermal aging process. The specific conclusions are as follows:

(1) Torsional loads weaken the physical crosslinking and entanglement between EPR molecules, increasing molecular activity and making them more susceptible to discharge particle bombardment and oxidation in the environment, thereby promoting oxidation. In addition, torsional stress causes molecular chains to shift, slide against each other, and break, increasing the occurrence of chain scission reactions.

(2) Torsional stress accelerates the fracture of chemical bonds and oxidation reactions by disrupting hydrogen bonds and weakening intermolecular entanglement. This results in the formation of more C–O or C=O groups, and the increased oxidation and chain scission reactions reduce the material's crystallinity, further impacting the mechanical performance of the cable.

(3) Nonlinear torsion leads to the generation of more small molecular groups and oxidation products in the samples under electrothermal aging. The increased polar molecules raise the conductivity, exacerbating the increase in the dielectric loss factor of EPR and accelerating the deterioration of the cable's insulation performance.

(4) Prolonged torsional stress on the cable may cause the outer sheath and insulation layer to crack due to fatigue

stress, promoting thermal oxygen permeation into the insulation, accelerating oxidation reactions in the insulation layer, which, in turn, leads to a decline in mechanical performance.

AUTHOR DECLARATIONS

Conflict of Interest

The authors have no conflicts to disclose.

Author Contributions

Shuaibing Li: Conceptualization (equal); Formal analysis (equal); Funding acquisition (equal); Methodology (equal); Supervision (equal); Writing – original draft (equal); Writing – review & editing (equal). **Baopeng Lu**: Conceptualization (equal); Investigation (equal); Methodology (equal); Validation (equal); Visualization (equal); Writing – original draft (equal); Writing – review & editing (equal). **Yi Cui**: Formal analysis (equal); Methodology (equal); Validation (supporting); Writing – review & editing (equal). **Yongqiang Kang**: Formal analysis (equal); Supervision (supporting); Validation (supporting). **Haiying Dong**: Supervision (supporting); Writing – review & editing (supporting).

DATA AVAILABILITY

The data that support the findings of this study are available from the corresponding author upon reasonable request.

REFERENCES

[1] Z. Lei, J. Song, M. Tian *et al.*, "Partial discharges of cavities in ethylene propylene rubber insulation," IEEE Trans. Dielectr. Electr. Insul. **21**(4), 1647–1659 (2014).

[2] L. Lin, C. Lin, P. Geng *et al.*, "Aging life evaluation of coal mining flexible EPR cables under multi-stresses," IEEE Access **8**, 53539–53546 (2020).

[3] W. Li, J. Li, X. Wang *et al.*, "Physicochemical origin of space charge dynamics for aged XLPE cable insulation," IEEE Trans. Dielectr. Electr. Insul. **21**(2), 809–820 (2014).

[4] S. Li, B. Cao, J. Li *et al.*, "Review of condition monitoring and defect inspection methods for composited cable terminals," High Voltage **8**(3), 431–444 (2023).

[5] A. Setayeshmehr, I. Fofana, C. Eichler *et al.*, "Dielectric spectroscopic measurements on transformer oil-paper insulation under controlled laboratory conditions," IEEE Trans. Dielectr. Electr. Insul. **15**(4), 1100–1111 (2008).

[6] L. Bai, M. Su, L. Sun *et al.*, "Mechanism characterization and nondestructive inspection method of thermal degradation faults in EPDM cable termination," IEEE Trans. Instrum. Meas. **71**, 1–12 (2022).

[7] X. Meng, Z. Wang, and G. Li, "Nondestructive condition assessment techniques for the ethylene-propylene rubber cable," Res. Non-Destr. Eval. **28**(1), 45–59 (2017).

[8] R. S. A. Afia, E. Mustafa, and Z. Á. Tamus, "Condition monitoring of photovoltaic cables based cross-linked polyolefin insulation under combined accelerated aging stresses: Electrical and mechanical assessment," Energy Rep. **8**, 1038–1049 (2022).

06 August 2024 05:03:50

[9] J. Li, S. Liu, J. Xu *et al.*, "Research on current carrying capacity and temperature rise of 66 kV wind turbine cable with high thermal conductivity," J. Electr. Eng. **18**(1), 244–250 (2023).

[10] L. Zhou, L. Bai, J. Zhang *et al.*, "Measurement and diagnosis of PD characteristics of industrial cable terminations in extreme cold environment," IEEE Trans. Instrum. Meas. **70**, 1–11 (2021).

[11] G. Gao, S. Zhou, S. Yang *et al.*, "Accurate identification partial discharge of cable termination for high-speed trains based on wavelet transform and convolutional neural network," Electr. Power Syst. Res. **225**, 109838 (2023).

[12] W. Zhou, H. Cheng, B. Hui, J. Huang, Y. Hao, G. Liu, and L. Li, "Key process of the defection of PET buffer layer in XLPE power cable by a case study: Thermo-oxidative degradation," Eng. Failure Anal. **146**, 107131 (2023).

[13] H. Shrimathi, M. Mondal, and P. Mishra, "Simulation based electric stress estimation on silicone rubber polymeric insulators under multi-environmental conditions," Electr. Power Syst. Res. **214**(Part A), 108840 (2023).

[14] B. Du, C. Han, and Z. Li, "Effect of mechanical stretching on nonlinear conductivity and dielectrics breakdown strength of SiR/SiC composites," IEEE Trans. Dielectr. Electr. Insul. **28**(3), 996–1004 (2021).

[15] B. Du, J. Su, and T. Han, "Effects of mechanical stretching on electrical treeing characteristics in EPDM," IEEE Trans. Dielectr. Electr. Insul. **25**(1), 84–93 (2018).

[16] S. Li, B. Cao, Y. Cui *et al.*, "Terahertz-based insulation delamination defect inspection of vehicle cable terminals," IEEE Trans. Transp. Electrif. **9**(1), 1765–1774 (2023).

[17] Y. Liu and X. Wang, "Research on property variation of silicone rubber and EPDM rubber under interfacial multi-stresses," IEEE Trans. Dielectr. Electr. Insul. **26**(6), 2027–2035 (2019).

[18] Z. Zhang, J. Jin, J. Liu *et al.*, "Experiment and analysis on temperature vibration aging of XLPE cable line," High Voltage Eng. **44**(11), 3707–3712 (2018).

[19] D. Bouguedad, A. Mekhaldi, O. Jbara *et al.*, "Physico-chemical study of thermally aged EPDM used in power cables insulation," IEEE Trans. Dielectr. Electr. Insul. **22**(6), 3207–3215 (2015).

[20] A. Awwad, D. McDaniel, L. Lagos *et al.*, "Effect of temperature and aging duration on ethylene propylene diene monomer (EPDM) nonmetallic components used in caustic liquid waste transfer lines," Eng. Failure Anal. **128**, 105633 (2021).

[21] C. Lin, C. Chien, J. Tan *et al.*, "Chemical degradation of five elastomeric seal materials in a simulated and an accelerated PEM fuel cell environment," J. Power Sources **196**(4), 1955–1966 (2011).

[22] M. Alagar, S. A. Majeed, A. Selvaganapathi, and P. Gnanasundaram, "Studies on thermal, thermal ageing and morphological characteristics of EPDM-g-VTES/LLDPE," Eur. Polym. J. **42**(2), 336–347 (2006).

[23] H. Wang, G. Tan, G. Yuri *et al.*, "Analysis of thermal aging life and physicochemical properties of crosslinked polyethylene seabed cable insulation," Polym. Mater. Sci. Eng. **31**(3), 71–75 (2015).

[24] K. Zhou, K. Li, M. Yang *et al.*, "Understanding electrical performance and microstructure of water tree aged cables after silicone injection during electrical-thermal accelerated aging," Electric Power Compon. Syst. **45**(12), 1370–1380 (2017).

[25] Z. Zhang, S. Meng, R. Xia *et al.*, "Experimental study on aging characteristics of XLPE insulation under vibration loads," High Voltage Eng. **42**(8), 2399–2405 (2016).

[26] Y. Liu, H. Liu, L. Yu *et al.*, "Effect of thermal stress on the space charge distribution of 160 kV HVDC cable insulation material," IEEE Trans. Dielectr. Electr. Insul. **24**(3), 1355–1364 (2017).

[27] X. Chen, A. R. Mantsch, L. Hu *et al.*, "Electrical treeing behavior of DC and thermally aged polyethylenes utilizing wire-plane electrode geometries," IEEE Trans. Dielectr. Electr. Insul. **21**(1), 45–52 (2014).

[28] H. Li, J. Li, Y. Ma *et al.*, "Effects of thermal aging on the crystal structures of the XLPE cable insulating material at different temperatures," Proc. CSEE **37**(22), 6740–6748+6787 (2017).

[29] G. Lian, "Design of high-load current-resistant and torsion-resistant power cables for offshore wind turbine units," Opt. Fiber Electric Cable Appl. **23**(4), 38–40 (2020).

[30] Y. Liu, X. Wang, and J. Chen, "Performance change and failure mechanism of ethlene propylene-diene monomer under interfical multi-stresses," J. Xi'an Jiaotong Univ. **53**(10), 86–95 (2019).

[31] F. G. Bonifacich, E. D. V. Giordano, O. A. Lambri *et al.*, "Study of dielectric strength in EPDM by nondestructive dynamic mechanical analysis in high electrical field," IEEE Trans. Dielectr. Electr. Insul. **24**(3), 1840–1851 (2017).

06 August 2024 05:03:50